

## **SIMULATIONS OF AEROELASTICITY IN AN ANNULAR CASCADE USING A PARALLEL 3-DIMENSIONAL NAVIER-STOKES SOLVER**

**Ivan McBean**  
 Department of  
 Mechanical Engineering  
 Monash University  
 Clayton, 3800  
 Australia

**Feng Liu**  
 Department of  
 Mechanical and Aerospace Engineering  
 University of California  
 Irvine, California 92697-3975

**Kerry Hourigan**  
**Mark Thompson**  
 Department of  
 Mechanical Engineering  
 Monash University  
 Clayton, 3800  
 Australia

### **ABSTRACT**

A parallel multi-block Navier-Stokes solver with the  $k-\omega$  turbulence model is developed to simulate the 3-dimensional unsteady flow through an annular turbine cascade. Results at mid-span are compared with the experimental results of Standard Test Case 4. Comparisons are made between 3-dimensional and 2-dimensional, and inviscid and viscous simulations. The inclusion of a viscous flow model does not greatly affect the stability of the configuration.

### **NOMENCLATURE**

$b_c$  magnitude of blade displacement non-dimensionalised with chord  
 $C_p$  Surface steady pressure coefficient  
 $C_{p(n)}$   $n$ th mode of surface unsteady pressure coefficient  
 $c$  blade chord  
 $E$  total energy per unit mass  
 $e$  internal energy per unit mass  
 $H$  total enthalpy per unit mass  
 $h$  enthalpy per unit mass  $e + p/\rho$   
 $k$  turbulence mixing energy  
 $k_c$  reduced frequency  
 $Pr_L$  laminar Prandtl number  
 $Pr_T$  turbulence Prandtl number  
 $p_1$  static pressure at inlet  
 $p_{01}$  total pressure at inlet

$P_{(n)}$   $n$ th mode of unsteady pressure  
 $p$  pressure  
 $t$  time  
 $u, v, w$  velocity components in the  $x, y$  and  $z$  directions  
 $\bar{u}, \bar{v}, \bar{w}$  relative velocity components  
 $x, y, z$  spatial velocity components  
 $\phi_{p(n)}$  phase  $n$ th mode of unsteady pressure  
 $\mu$  molecular viscosity  
 $\mu_T$  turbulence eddy viscosity  
 $\rho$  density  
 $\omega$  turbulence specific dissipation rate  
 $\gamma$  ratio of specific heats  
 $\Xi$  damping coefficient

### **INTRODUCTION**

With the development of computers, increasingly complex models have been generated to reproduce the aeroelastic response in turbomachinery.

There have been a large number of 2-dimensional studies into the phenomenon of aeroelasticity in turbomachinery and these have been referenced in a number of review papers (Imregun, 1998; Srinivasan, 1997; Marshall & Imregun, 1996; Verdon, 1993). However the importance of 3-dimensional and viscous effects in the fluid blade coupling and the ability of 3-dimensional viscous simulations to model unsteady aerodynamics has only

been investigated by a limited number of researchers. The unsteady Navier-Stokes equations with a linearised  $k-\omega$  turbulence model has been applied the 2-dimensional Standard Test Case 10 that involves separated flow (Holmes & Lorence, 1998). The analysis of a bird-damaged fan assembly has been investigated using the Navier-Stokes equations with a one-equation Baldwin-Barth turbulence model and a coupled approach (Ferrari *et al.*, 1999). The thin-layer Navier-Stokes equations (Marshall & Imregun, 1996) and viscous loss models (Sayma *et al.*, 1998) have been used to approximate the unsteady viscous effects in order to reduce computation time. Euler simulations of turbomachinery aeroelasticity have also been performed for 3-dimensional configurations (Gerolymos & Vallet, 1996; Chuang & Verdon, 1999). The majority of these investigations have concentrated on the ability of the simulation to predict the stability of a configuration rather than a direct comparison of the unsteady aerodynamics with experimental measurements.

In general, computational studies of unsteady aerodynamics require resources that are well beyond a single processor. However the development of multiple processor systems has greatly increased computational speed through the calculation of problems in parallel. The solution of field and fluid problems lend themselves easily to solution in parallel, as the computational domain may be divided into blocks and the field equations solved for on separate processors. A 3-dimensional and unsteady Navier Stokes code has been developed from a code that calculated the steady state solution for single blade passages in turbine cascades (Liu & Jameson, 1993; Liu & Zheng, 1994; Liu & Zheng, 1996; Liu *et al.*, 1998). The new implementation includes an unsteady solver, moving grid, multiple processor capability and structural model.

Few 3-dimensional experimental measurements exist in the field of unsteady aerodynamics in turbomachinery. A large effort has been made to compile measurements for oscillating cascades that are typical of those found in industry through the Workshop on Aeroelasticity in Turbomachines (Bölcs & Fransson, 1986), however measurements in these cases are made at mid span and blade motion is symmetric in the radial plane to minimise the 3-dimensional effects on results.

The Standard Test Case 4 is described as a highly loaded turbine rotor, involving typical sections of modern free standing turbine blades (Bölcs & Fransson, 1986). The flow is high subsonic and the blade normally exhibits flutter in the first bending mode. To simulate the unsteady flow, the blade is forced to oscillate in this bending mode by translation at an angle to the axial axis in the radial plane. Viscous effects in two dimensional models have been simulated numerically for this case by other authors using the Navier-Stokes equations with the algebraic Baldwin Lomax Model (Grueber & Carstens, 1998) and the  $k-\omega$  turbulence model (Ji & Liu, 1999).

Recently, complete conditions at the cascade inlet and outlet plane have been made available for Standard Test Case 4. This

allows the authors to validate the 3-dimensional implementation and investigate the difference between a number of different cascade models. Blade stability will be calculated by way of the energy method.

### Cascade Model

There are two different geometric configurations considered. The first is a 2-dimensional cascade model where the dimensions of the 2-dimensional slice are taken to be at mid-span of the experiment. The second involves 3-dimensional annular passages. The inlet and outlet plane lies one chord upstream and downstream of the blade's leading and trailing edges, respectively.

Lane's (Lane, 1956) travelling wave model is used where a single vibrational mode shape is considered, with an inter-blade-phase-angle (IBPA) assumed between adjacent blade passages. Since there are a finite number of possible IBPA's for a rotor of finite radius, only a limited number are required. In the numerical simulation, the annular or linear cascade is truncated at the lowest number of passages required and periodicity is assumed at the boundaries of the cascade. As many passages are required to repeat the flow pattern and vibration mode shape.

The frequency of vibration is specified as a reduced frequency,

$$k_c = \frac{c\omega}{2U_{ref}}$$

where  $U_{ref}$  is the magnitude of the flow velocity at the outlet. Steady and unsteady surface pressure coefficients are referenced to the inlet static pressure,

$$C_p = \frac{p - p_1}{p_{01} - p_1},$$

$$C_{p(n)} = \frac{p_{(n)}}{b_c(p_{01} - p_1)}.$$

The energy method is applied to determine the stability of a particular configuration. The unsteady aerodynamic work coefficient is integrated over the entire blade for a cycle of oscillation. This quantity is transformed to the frequency domain using a fast Fourier transform. Since the signal is almost purely sinusoidal, there is a single dominant mode. This mode is regarded as a complex number and the phase of the forcing function is zero, therefore the imaginary part of the work function, also known as the damping coefficient, may be used to indicate the stability of the configuration. A negative coefficient is stable – the forcing function leads the forcing of the blade and the motion is damped. If the coefficient is positive, the forcing of the blade leads the displacement function and thus adds energy to the system and the system is unstable.

For the 3-dimensional simulations the radial distribution of inlet quantities of total pressure, total temperature and flow angle are prescribed, while at the outlet the radial distribution of pressure is prescribed. At the periodic boundaries, velocities are rotated through the appropriate angle for the annular case.

$$\mathbf{g} = \begin{pmatrix} \rho \bar{v} \\ \rho u \bar{v} \\ \rho v \bar{v} + p \\ \rho w \bar{v} \\ \rho E \bar{v} + p v \\ \rho k \bar{v} \\ \rho \omega \bar{v} \end{pmatrix}, \quad \mathbf{h} = \begin{pmatrix} \rho \bar{w} \\ \rho u \bar{w} \\ \rho v \bar{w} \\ \rho w \bar{w} + p \\ \rho E \bar{w} + p w \\ \rho k \bar{w} \\ \rho \omega \bar{w} \end{pmatrix},$$

## Governing Equations and Numerical Method

The fluid field equations solved are the 3-dimensional, Favre averaged Navier-Stokes equations coupled with the energy equation and Wilcox's (Wilcox, 1988)  $k-\omega$  turbulence model for closure. These are discretized on a structured hexahedral grid using the finite volume representation. The artificial dissipation of Jameson (Jameson *et al.*, 1981) is implemented. The  $k-\omega$  turbulence model is solved in a similar manner on the same finite volume mesh with some of the terms treated implicitly to aid convergence and stability (Liu & Zheng, 1994; Zheng & Liu, 1995; Liu & Zheng, 1996). The turbulence model scheme was changed from cell vertex to cell centre due to message passing and stability issues. Both sets of equations are solved explicitly in a coupled manner through a 5 stage Runge Kutta scheme. The time accurate unsteady solution is found through Jameson's fully implicit dual time stepping scheme (Jameson, 1991; Alonso & Jameson, 1994; Alonso, 1997).

The fluid governing equations can be written in integral form over a fixed control volume  $\Omega$  as

$$\begin{aligned} & \frac{\partial}{\partial t} \iint_{\Omega} \mathbf{w} d\Omega + \oint \mathbf{f} dS_x + \mathbf{g} dS_y + \mathbf{h} dS_z \\ &= \oint \mathbf{f}_\mu dS_x + \mathbf{g}_\mu dS_y + \mathbf{h}_\mu dS_z + \iint_{\Omega} \mathbf{S} d\Omega \end{aligned} \quad (1)$$

where  $\mathbf{w}$  include the conservative variables for mass, momentum, energy, turbulent kinetic energy and turbulent specific dissipation rate;  $\mathbf{f}$ ,  $\mathbf{g}$  and  $\mathbf{h}$  are the convective flux vectors;  $\mathbf{f}_\mu$ ,  $\mathbf{g}_\mu$  and  $\mathbf{h}_\mu$  are the diffusive flux vectors; and  $\mathbf{S}$  is a volume source term. These are given by

$$\mathbf{w} = \begin{pmatrix} \rho \\ \rho u \\ \rho v \\ \rho w \\ \rho E \\ \rho k \\ \rho \omega \end{pmatrix}, \quad \mathbf{f} = \begin{pmatrix} \rho \bar{u} \\ \rho u \bar{u} + p \\ \rho v \bar{u} \\ \rho w \bar{u} \\ \rho E \bar{u} + p u \\ \rho k \bar{u} \\ \rho \omega \bar{u} \end{pmatrix},$$

$$\mathbf{f}_\mu = \begin{pmatrix} 0 \\ \hat{\tau}_{xx} \\ \hat{\tau}_{yx} \\ \hat{\tau}_{zx} \\ u \hat{\tau}_{xx} + v \hat{\tau}_{yx} + w \hat{\tau}_{zx} + (\mu + \sigma^* \mu_T) \frac{\partial k}{\partial x} - q_x \\ (\mu + \sigma^* \mu_T) \frac{\partial k}{\partial x} \\ (\mu + \sigma \mu_T) \frac{\partial \omega}{\partial x} \end{pmatrix},$$

$$\mathbf{g}_\mu = \begin{pmatrix} 0 \\ \hat{\tau}_{xy} \\ \hat{\tau}_{yy} \\ \hat{\tau}_{zy} \\ u \hat{\tau}_{xy} + v \hat{\tau}_{yy} + w \hat{\tau}_{zy} + (\mu + \sigma^* \mu_T) \frac{\partial k}{\partial y} - q_y \\ (\mu + \sigma^* \mu_T) \frac{\partial k}{\partial y} \\ (\mu + \sigma \mu_T) \frac{\partial \omega}{\partial y} \end{pmatrix},$$

$$\mathbf{h}_\mu = \begin{pmatrix} 0 \\ \hat{\tau}_{xz} \\ \hat{\tau}_{yz} \\ \hat{\tau}_{zz} \\ u \hat{\tau}_{xz} + v \hat{\tau}_{yz} + w \hat{\tau}_{zz} + (\mu + \sigma^* \mu_T) \frac{\partial k}{\partial z} - q_z \\ (\mu + \sigma^* \mu_T) \frac{\partial k}{\partial z} \\ (\mu + \sigma \mu_T) \frac{\partial \omega}{\partial z} \end{pmatrix},$$

$$\mathbf{S} = \begin{pmatrix} 0 \\ 0 \\ 0 \\ 0 \\ \tau_{ij} \frac{\partial u_i}{\partial x_j} - \beta^* \rho \omega k \\ \frac{\alpha \omega}{k} \tau_{ij} \frac{\partial u_i}{\partial x_j} - \beta \rho \omega^2 \end{pmatrix}. \quad (2)$$

In the above equations,  $t$  is time,  $\rho$  density,  $p$  pressure,  $\mu$  molecular viscosity,  $k$  turbulent mixing energy, and  $\omega$  the specific dissipation rate. Subscripts  $i = 1, 3$  indicate the three coordinate

directions. Quantities  $x_i$ , or  $x$ ,  $y$  and  $z$ , stand for the position vectors and  $u_i$ , or  $u$ ,  $v$  and  $w$ , are the flow velocity components in the  $x$ ,  $y$  and  $z$  directions. The total energy and enthalpy are defined  $E = e + k + u_i u_i / 2$  and  $H = h + k + u_i u_i / 2$ , respectively, with  $h = e + p/\rho$ , and  $e$  is the internal energy. Other quantities are defined in the following equations:

$$\mu_T = \alpha^* \frac{\rho k}{\omega} \quad (3)$$

$$S_{ij} = \frac{1}{2} \left[ \frac{\partial u_i}{\partial x_j} + \frac{\partial u_j}{\partial x_i} \right] \quad (4)$$

$$\tau_{ij} = 2\mu_T \left[ S_{ij} - \frac{1}{3} \frac{\partial u_k}{\partial x_k} \delta_{ij} \right] - 2/3 \rho k \delta_{ij} \quad (5)$$

$$\hat{\tau}_{ij} = 2\mu \left[ S_{ij} - \frac{1}{3} \frac{\partial u_k}{\partial x_k} \delta_{ij} \right] + \tau_{ij} \quad (6)$$

$$q_j = -C_p \left( \frac{\mu}{Pr_L} + \frac{\mu_T}{Pr_T} \right) \frac{\partial T}{\partial x_j} \quad (7)$$

where  $Pr_L$  and  $Pr_T$  are the laminar and turbulent Prandtl numbers, respectively. The molecular viscosity,  $\mu$ , is calculated by Sutherland's law.  $\beta$ ,  $\beta^*$ ,  $\alpha$ ,  $\alpha^*$ ,  $\sigma$ , and  $\sigma^*$  are closure parameters for the  $k-\omega$  turbulence model.

A dual time stepping scheme (Jameson, 1991) is used to calculate the unsteady flow problem. A second order accurate, fully implicit scheme is used to evolve the unsteady problem in a time accurate manner.

## Parallel Implementation

Domain decomposition is used to sub-divide each blade passage into a number of blocks. The Message Passing Interface (MPI) is used to implement the parallel code. Both flow and turbulence model quantities are passed at block boundaries. Within the code each block is considered a single entity – only boundary information is required. The two equation turbulence model requires only local knowledge of the flowfield, unlike some algebraic models that require global length scale calculations to maintain continuity over block boundaries.

A high level of Fortran90 is implemented and flowfield quantities are considered as high level objects. In the application of boundary conditions, a transformation is used for the

coordinate system so that each routine is written for one set of coordinates only. The flow and geometric quantities for the multiple grids within the multigrid solver are also regarded as objects, with residuals and the flow field interpolated between these blocks.

The moving grid is implemented through transfinite interpolation within each computational block. This method is highly efficient and requires less computational work than regenerating the grid completely at every time step. Moving faces attached to the blade are assigned a blade number and from this is assigned a phase for the prescribed oscillation. These are collected on the root processor and at every real time step the grid is adapted to the new position of the blades. The moving grid method has been successfully applied to the modelling of aeroelasticity in wings (Wong *et al.*, 2000; Liu *et al.*, 2000) and in two dimensional analysis of turbine aeroelasticity (Sadeghi & Liu, 2000). Details of the method and its implementation have been previously presented (Wong *et al.*, 2000).

## Results and Discussion

Inviscid and Navier-Stokes simulations were performed for both 2-dimensional and 3-dimensional configurations of Standard Test Case 4. Within Test Case 4 there are a number of measurements; results here are compared with Test 627. In this case, the passage flow was in the high sub-sonic regime with a reduced frequency of  $k_c = 0.1187$  and involving a bending amplitude of  $b_c = 3.8 \times 10^{-3}$ . At the inlet  $Ma_{in} = 0.18$  and at the outlet  $Ma_{out} = 0.9$ . It was found that using the present method about 4 oscillations were required for a converged unsteady solution as described in previous work (Ji & Liu, 1999).

The grid convergence of the  $k-\omega$  simulations was only performed for 2-dimensional configurations. It was found that a mesh of  $160 \times 64$  was sufficient to provide grid convergence with a  $y^+ < 3$  at mid-chord on the suction side. A finer grid with a  $y^+ < 1$  was also used, however this produced a variation in the steady pressure coefficient of less than 1 percent. The number of cells was doubled in the axial direction but this made little difference to the steady surface pressure coefficient. With the typical mesh, a half an order of magnitude change in the smallest cell size at the boundary resulted in less than 1 percent variation in the surface pressure coefficient. Based on the 2-dimensional grid convergence studies, a mesh of  $160 \times 64 \times 64$  is used for 3-dimensional Navier-Stokes simulations. The largest grid involved approximately 2.6 million points spread over 32 computational blocks. A typical mesh for a four passage, 3-dimensional Euler simulation is shown in Figure 1.

The steady pressure coefficient is shown for both the 2-dimensional and 3-dimensional cascades in Figure 2. The 2-dimensional Euler and Navier-Stokes agree well with other authors. However the 3-dimensional results vary for both flow models. The  $k-\omega$  results under-predict the suction over the back

portion of the blade suction side, while the inviscid result under-predicts the suction in the mid-chord region. The reason for this deviation is not obvious, although it should be noted that the grid resolution study was only performed for the 2-dimensional case.

A comparison of the unsteady pressure coefficient for an inter-blade phase angle of 180 degrees is shown in Figure 3. For the 3-dimensional results, the pressure coefficient is taken at mid-span. The Euler results differ from the Navier-Stokes calculations; this is probably due to the lack of blockage due to the viscous boundary layer. There is some deviation amplitude at quarter chord, however these were also observed in 2-dimensional simulations by other authors (Grueber & Carstens, 1998) and as yet is unexplained. There is a large difference in the predictions of the distribution of phase angle for the surface pressure coeffi-

cient, in particular for the suction side region between mid-chord and the trailing edge. The experimental measurements of phase for this region for the configuration are very different from those presented earlier (Bölcs & Fransson, 1986) and the numerical results for phase compare well with those for the slightly different flow conditions by other authors (Grueber & Carstens, 1998). On the suction side, the phase is closest to the experimentally measured value where the magnitude of the unsteady pressure coefficient is highest.

There is good agreement between the 2-dimensional and 3-dimensional models. Figure 4 shows similar results for an IBPA of 90 degrees; the inviscid result drops below the viscous one at mid chord – it is assumed that this is once again due to the blockage of the boundary layer.

The unsteady results were investigated along the span of the blade, as shown in Figure 5. The effects of the passage vortices on the unsteady pressure coefficient appear minimal and the coefficient on the suction side collapses onto each other toward the trailing edge. However at 10 percent span for the inviscid result, the suction side pressure deviates from the viscous results. Un-

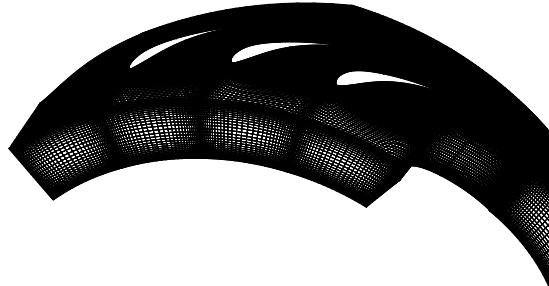


Figure 1. Typical mesh for a four passage, 3-dimensional Euler simulation.

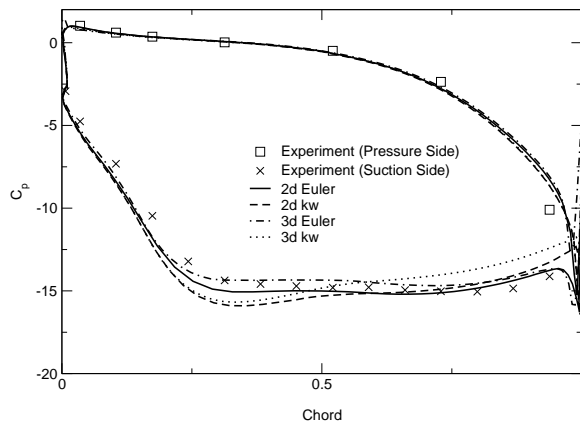


Figure 2. Steady surface pressure coefficient.

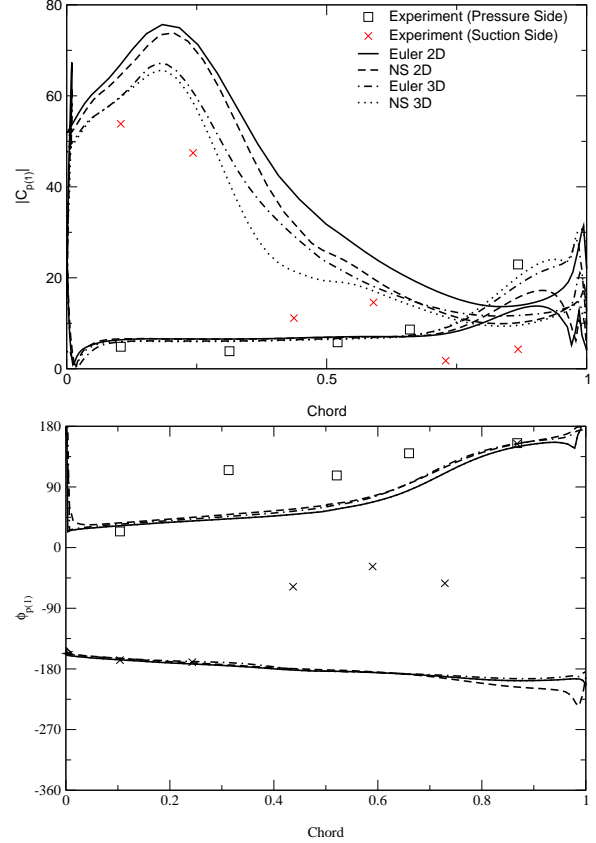


Figure 3. Comparison of different models for first mode of unsteady pressure coefficient for IBPA=180.

steady pressure coefficients in this figure are referenced to the static pressures at the mid-span of the passage inlet.

Blade surface pressures were integrated over the displacement cycle to gauge the stability of the configuration, using the energy method. Results are shown in Figure 6. A positive damping coefficient indicates a stable configuration and conversely a negative coefficient is unstable. A description of the calculation of this quantity is also provided in Böös and Fransson (1986).

It is interesting to note that the different unsteady pressure coefficients of the various models produce similar damping coefficients. Even though the experiment involved six pressure taps on each blade surface, it provided sufficient resolution to compare well with the simulations.

Uncertainty remains regarding the condition of the inlet boundary layer, and the condition of the blade boundary layers. The present simulation has assumed fully turbulent walls. However it is believed that refinements will not alter the stability predictions to a large degree.

## Conclusions

A parallel unsteady 3-dimensional Navier-Stokes code with a two-equation turbulence model has been developed to simulate unsteady flows through oscillating turbomachinery blade rows. Although the 3-dimensional simulations tend to over-predict the amplitude of the unsteady pressure oscillation, there is reasonable agreement with experiment on the overall behaviour in the unsteady pressure distributions and aerodynamics damping coefficients.

The purpose of this paper is to document unsteady aeroelastic simulation results, especially effects due to 3-dimensionality and viscosity, by a multi-block 3-dimensional Navier-Stokes code with the  $k-\omega$  two equation turbulence model. Computations of the Standard Test Case 4, however, show only small differences between results by the 3-dimensional viscous code and 2-dimensional inviscid solutions, indicating that this is essentially 2-dimensional and viscous effects are not important on the flutter stability for this case. Further investigations are required to examine cases where viscous effects such as tip gap leakage and flow separation may have a greater influence on

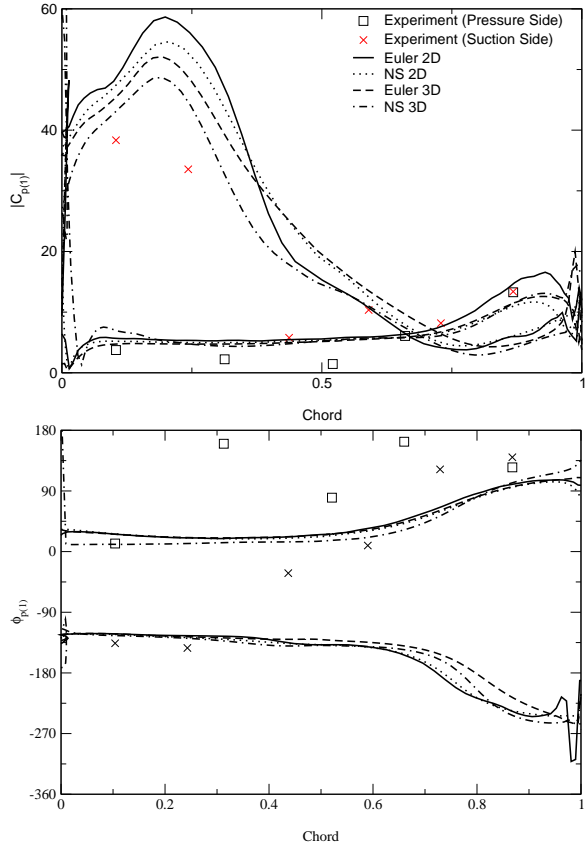


Figure 4. Comparison of different models for first mode of unsteady pressure coefficient for IBPA=90.

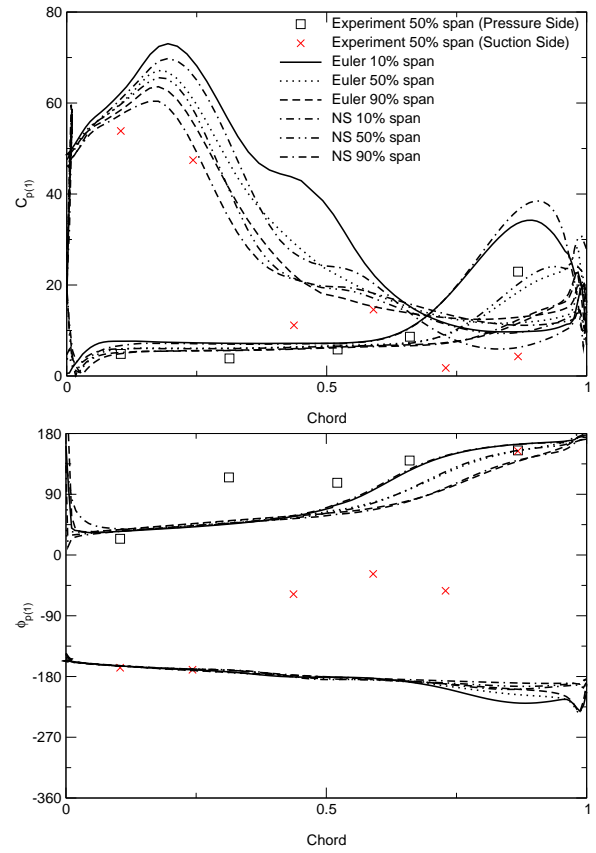


Figure 5. Comparison of unsteady pressure coefficient at different spanwise locations for 3D model for IBPA=180.

aeroelastic stability.

## Acknowledgments

The authors wish to thank VPAC for the use of the state facility Compaq Alpha in Melbourne and APAC for the use of the national facility Compaq Alpha in Canberra under project d93 in the merit allocation scheme.

## References

- Alonso, Juan, & Jameson, Antony. 1994 (Jan.). Fully-implicit time-marching aeroelastic solutions. *In: AIAA 32nd Aerospace Sciences Meeting*. AIAA. 94-0056.
- Alonso, Juan Jose. 1997 (June). *Parallel computation of unsteady and aeroelastic flows using an implicit multigrid-driven algorithm*. Ph.D. thesis, Princeton University.
- Bölcs, A., & Fransson, T. H. 1986. *Aeroelasticity in turbomachines: Comparison of theoretical and experimental cascade results*. Lausanne: EPFL.
- Chuang, H. A., & Verdon, J. M. 1999. A nonlinear simulator for three-dimensional flows through vibrating cascades. *ASME Journal of Turbomachinery*, **121**(Apr.), 348–357.
- Ferrari, E., Vahdati, M., & Imregun, M. 1999 (Mar.). Flutter stability of a bird-damaged fan assembly. *Pages 365–376 of: IMech Conference Transactions*. 3rd European Conference on Turbomachinery. C557/116/99.
- Gerolymos, G. A., & Vallet, I. 1996. Validation of three-dimensional Euler methods for vibrating cascade aerodynamics. *Journal of Turbomachinery*, **118**, 771–782.
- Grueber, B., & Carstens, V. 1998. Computation of the unsteady transonic flow in harmonically oscillating turbine cascades taking into account viscous effects. *Journal of Turbomachinery*, **120**(Jan.), 104–111.
- Holmes, D. G., & Lorence, C. B. 1998. Three dimensional linearized Navier Stokes calculations for flutter and forced response. *Pages 211–224 of: Fransson, T. (ed), Unsteady Aerodynamics and Aeroelasticity of Turbomachines*. Kluwer Academic Publishers.
- Imregun, M. 1998. Recent developments in turbomachinery aeroelasticity. *Computational Fluid Dynamics '98*, 524–533.
- Jameson, A., Schmidt, W., & Turkel, E. 1981 (June). Numerical solutions of the Euler equations by finite volume methods using Runge-Kutta time-stepping schemes. *In: AIAA 14th Fluid and Plasma Dynamics Conference*. AIAA.
- Jameson, Antony. 1991 (June). Time dependent calculations using multigrid, with applications to unsteady flows past airfoils and wings. *In: AIAA 10th computational fluid dynamics conference*. AIAA.
- Ji, Shanhong, & Liu, Feng. 1999. Flutter computation of turbomachinery cascades using a parallel unsteady Navier-Stokes code. *AIAA Journal*, **37**(3), 320–327.
- Lane, Frank. 1956. System mode shapes in the flutter of compressor blade rows. *Journal of the Aeronautical Sciences*, Jan., 54–66.
- Liu, F., Cai, J., Zhu, Y., & A. S. F. Wong, H. M. Tsai. 2000 (Jan.). Calculation of wing flutter by a coupled CFD-CSD method. *In: AIAA 38th Aerospace Sciences Meeting & Exhibit*. AIAA. AIAA 2000-0907.
- Liu, Feng, & Jameson, Antony. 1993. Multigrid Navier-Stokes calculations for three-dimensional cascades. *AIAA Journal*, **31**(10), 1785–1791.
- Liu, Feng, & Zheng, Xiaoqing. 1994. Staggered finite volume scheme for solving cascade flow with a  $k-\omega$  turbulence model. *AIAA Journal*, **32**(8), 1589–1597.
- Liu, Feng, & Zheng, Xiaoquing. 1996. A strongly coupled time-marching method for solving the Navier-Stokes and  $k-\omega$  turbulence model equations with multigrid. *Journal of Computational Physics*, **128**, 289–300.
- Liu, Feng, Jennions, Ian K., & Jameson, Antony. 1998 (Jan.). Computation of turbomachinery flow by a convective-upwind-split-pressure (CUSP) scheme. *In: 36th Aerospace Sciences Meeting and Exhibit*. AIAA.
- Marshall, J. G., & Imregun, M. 1996 (June). An analysis of the aeroelastic behavior of a typical fan-blade with emphasis on the flutter mechanism. *In: International Gas Turbine and Aeroengine Congress and Exhibition*. ASME. 96-GT-78.
- Sadeghi, M., & Liu, F. 2000 (Jan.). Computation of mistuning effects on cascade flutter. *In: AIAA 38th Aerospace Sciences Meeting & Exhibit*. AIAA. AIAA 2000-0230.
- Sayma, A., Vahdati, M., Green, J., & Imregun, M. 1998. Whole-assembly flutter analysis of a low pressure turbine blade. *Pages 347–359 of: Fransson, T. (ed), Unsteady Aerodynamics and Aeroelasticity of Turbomachines*. Kluwer Academic Publishers.

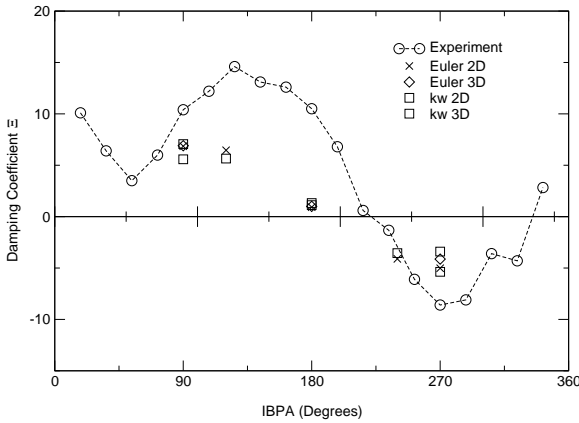


Figure 6. Damping coefficient for different configurations over a range of inter-blade-phase-angles.

- Srinivasan, A. V. 1997. Flutter and resonant vibration characteristics of engine blades. *Journal of Engineering for Gas Turbines and Power*, **119**(Oct.).
- Verdon, Joseph. 1993. Review of unsteady aerodynamic methods for turbomachinery aeroelastic and aeroacoustic applications. *AIAA Journal*, **31**(2), 235–250.
- Wilcox, D. C. 1988. Reassessment of the scale-determining equation for advanced turbulence models. *AIAA Journal*, **26**(11), 1299–1310.
- Wong, A. S. F., Tsai, H. M., Cai, J., Zhu, Y., & Liu, F. 2000 (Jan.). Unsteady flow calculations with a multi-block moving mesh algorithm. In: *38th Aerospace Sciences Meeting and Exhibit*. AIAA. AIAA-2000-1002.
- Zheng, Xiaoqing, & Liu, Feng. 1995. Staggered finite volume scheme for solving Navier-Stokes and k- $\omega$  turbulence model equations. *AIAA Journal*, **33**(6), 991–998.